Title
Revealing the diversity of hydropeaking flow regimes

Authors
Li, Tingyu
Pasternack, Gregory B

Publication Date
2021-07-01

DOI
10.1016/j.jhydrol.2021.126392

Data Availability
The data associated with this publication are available upon request.

Peer reviewed

Revealing the diversity of hydropeaking flow regimes

Tingyu Li[a*], Gregory B. Pasternack[a]
Department of Land, Air and Water Resources, University of California, Davis, United States
*Corresponding author: styli@ucdavis.edu

Cite as: Li, T., Pasternack G. B. 2021. Revealing the diverse pattern of hydropeaking flow. Journal of Hydrology 598: 126392. DOI. 10.1016/j.jhydrol.2021.126392.

Abstract

Hydropeaking, a hydroelectricity generation strategy involving rapid changes to flow releases from dams in response to fluctuations in hourly-adjusted electricity markets has been widely applied due to its economic efficiency. However, these operational practices produce sub-daily flow fluctuations that pose substantial hazards to riverine ecosystems and human activities. To ascertain the downstream impacts of hydropeaking, features of hydropeaking have been analyzed with respect to ecologically relevant hydrologic variables. However, since studies aiming to characterize hydropeaking regime often require manual feature extraction, they are limited to small temporal and spatial scales. Additionally, riverine ecologists have commonly treated hydropeaking as a broadly similar flow-alteration pattern regardless of the complexities of the electricity market and differences in the natural settings where it is applied. Therefore, this study sought to determine whether significantly different hydropeaking patterns exist on a regional scale, as revealed by the variation in hydropeaking over a long temporal scale (> five years). To fulfill this goal, a new algorithm, the Hydropeaking Event Detection Algorithm (HEDA), was developed in R to automate the characterization of hydropeaking flow regimes. Clustering analyses were conducted to explore the similarities and differences of hydropeaking regimes among 33 sites in numerous hydrologic regions of California. Four distinct classes of hydropeaking flow regimes were identified and distinguished by the duration and frequency of hydropeaking. Meanwhile, rate of change, amplitude and timing of hdyropeaking played less important roles in the classification.

Keywords: hydropeaking, automated feature extraction, clustering analysis, environmental flow.

1 Introduction

Hydropeaking operation is widely implemented due to the real-time electricity market mechanism and hydropower's ability to quickly respond to peak electricity demands (Moog 1993). Rapid flow fluctuation is one of the most significant disturbances caused by hydropeaking power plants and summarized as frequent, large and rapid flow fluctuations, occurring as one or several peaks per day with certain periodicity (Meile et al. 2011, Charmasson and Zink. 2011, Poff and Schmidt, 2016). Studies on hydropeaking started by comparing hydropeaking flow with natural flow to characterize the hydropeaking process, and to infer the critical condition when hydropeaking exceeds the ecological tolerance of river systems (Moog 1993, Poff and Ward, 1989, Young et al. 2011). These studies found that the magnitude, frequency, duration, timing and rate of change of hydropeaking significantly impact the age, growth, movement, migration, spawning and rearing of aquatic organisms (Reichstein et al. 2019, Harby et al. 2013, Anindito et al. 2019). For example, the relatively sudden flow decreases (rate of change-fall) can strand fish in isolated shallows and gravel-bar interstices as water level recedes (Hauer et al. 2017a, Hauer et al. 2017b, Melcher et al. 2017, Larrieu et al. 2021). Even though stranding may affect only a small portion of the fish population at a time, and may occur naturally, repeated flow fluctuations (frequency) can cause cumulative mortalities that can result in a significant fish loss (Young et al. 2011). Meanwhile, the ramping range (amplitude) of hydropeaking flow can partially explain the downstream displacement of both fish and macroinvertebrates (Thompson et al. 2011, Schülting et al. 2016). In addition, riparian plants face both physiological and physical constraints because of the shifts between submergence and drainage, and erosion of substrates (Bejarano et al. 2018). Nevertheless, most studies set natural flow as the reference condition and treat hydropeaking broadly similarly, which ignores the complexity of both power markets and natural settings (Haas et al. 2015, Lane et al. 2017). As a result, the general application in hydropeaking mitigation of these studies may be limited because each study can be site specific.

With an increasing understanding of the hydropeaking flow-ecology relationship, characterizing hydropeaking flow regimes systematically became an important topic. At the early stage, because of the availability of data and computation capability, only daily flow was used to evaluate hydropeaking-induced flow alteration which was found to mask features of hydropeaking flow.

Instead, sub-daily flow data was needed to properly assess hydropeaking-induced flow alteration and its ecological impacts (Zimmerman et al. 2010, Spurgeon et al. 2016). With sub-daily flow, the short-term changes in hydropeaking flow that used to be masked by the daily flow can now be described. For example, Bejarano et al. (2017) found that sub-daily flow magnitudes such as amplitude and rate of change made the largest differences between hydropeaking flow and natural flow regime. Beyond the general differences between natural flow and hydropeaking, the hydropeaking-induced flow variation was found to differ from each other. Carolli et al. (2015) set thresholds for normalized amplitude and rate of change of hydropeaking flow, and divided hydropeaking flow regimes into three groups to represent different degrees of pressure that hydropeaking-induced flow variation imposed on the downstream aquatic system. Greimel et al. (2016) listed different types of hydropeaking flow regimes differentiated by the hydropeaking intensity and types of hydropower facilities. In the United States, McManamay (2015) found that peaking operations were the most prevalent type of hydropower operation based on extensive documentation mining, and identified three specific types of hydropeaking operations: peaking, intermediate peaking and run-of-river peaking. All these findings inspire this study, whose objective is to advance our fundamental understanding of hydropeaking regimes by conducting an explicit, data-driven analysis exploring the possible patterns and diversity among hydropeaking flow regimes.

Hydrologic classification is the process of systematically arranging streams into groups that are most similar with respect to the characteristics or determinants of their flow regime (Olden et al. 2012). By identifying and categorizing dominant features (as revealed through a suite of hydrologic variables), hydrologic classification not only assists in describing the flow regimes at a regional scale but can also improve the predictive power and process basis of flow-ecology relationships. This ultimately leads to more effective environmental flow management with minimal data and resource requirements (Corduas 2011, Lane et al. 2018, Sergeant et al. 2020). Despite the marked value of hydrologic classification and rapidly growing computational power, limited hydrologic classification work on hydropeaking has been developed to characterize hydropeaking flow regimes at a regional scale (Palmer et al. 2005, Bergen et al. 2019, Reichstein et al. 2019). Part of the reason for this is that methods used to parse sub-daily hydropeaking flow are difficult to apply at a large spatial and temporal scale due to the frequent need to perform site pairing with gauging stations and feature extraction manually.

Approaches available for characterizing hydropeaking flow regimes have also constrained our understanding of hydropeaking-induced flow alteration. The Indicators of Hydrologic Alteration (IHA) and its derivatives have been used to characterize hydropeaking-induced flow fluctuations (Cushman 1985, Richter et al. 1996). However, when dealing with sub-daily flow records, IHA and its derivatives are incapable of capturing the time-series variation of the whole period because of the burdensome feature extraction. To address this issue, wavelet transforms have been applied to extract the spectral pattern of hydropeaking flow by fully considering time-series variation at different temporal resolutions (Daubechies 1992, Zolezzi et al. 2009, Wu et al. 2015). Nevertheless, wavelet transforms can only be applied to one stream at a time and results are difficult to interpret in terms of ecological implications. To address limitations of these two approaches, a new method was devised to integrate IHA into wavelet transform by replacing the original energy amplitude with the IHA index amplitude in the scale-averaged wavelet transform spectrum (Zolezzi et al. 2009). While this approach successfully fused the advantages of the two methods, it is still limited to the daily flow of an individual river. After that, an algorithm named COSH was developed to analyze the time-series variation of hydropeaking flow (Sauterleute and Charmasson, 2014). Even though COSH made an important advance in mining hydropeaking features automatically, iterative adjustments to thresholds are needed to detect hydropeaking events for each river. These leaves open a gap for highly automated methods that can process a large number of records and the need for more basic science to handle extensive flow records with a high temporal resolution across a hydrologically diverse region.

In this study, the goal was to explore the diversity of hydropeaking flow regimes at a regional scale. To fulfill this goal, a new algorithm was developed to (1) distinguish hydropeaking flow from non-hydropeaking flow, and (2) automate hydropeaking regime characterization by treating flow records as Euclidean vectors and identifying peaking events by vector angle and magnitude. The application of a dynamic threshold consists of daily maximum and minimum flow prevented this algorithm from requiring iterative, manual adjustments for different time windows and river reaches. The algorithm was applied to 128 sites with sub-daily flow records in California and identified 33 sites with hydropeaking signals. Then, hydrologic classification was applied to the identified 33 sites to classify the broad range of hydropeaking process (governed by the electricity demand, power transmission lines, electricity price and natural site constraints) into several discrete categories. Two types of clustering analyses, hierarchical and fuzzy clustering, were used to provide a clear structural interpretation of data that sheds light on the underlying organized patterns of hydropeaking flow while still considering the uncertainty of cluster membership.

2 Material and methods

2.1 Study sites

The study region comprises the state of California (425,000 km^2), a highly heterogeneous region with respect to physical and climatic characteristics. California contains both the highest (4,418 m) and lowest (-86 m) points in the contiguous U.S. and extends from 32° N to 42° N latitude. A 600-km north-south-oriented mountain range, the Sierra Nevada, situated in eastern California provides large natural potential energy for hydropower facilities. California primarily exhibits a Mediterranean climate with cold and wet seasons (October-May), and warm and dry season (June-September). Many rivers with hydropower facilities have their source in high-altitude zones of the Sierra Nevada, where most precipitation in winter has historically been stored as snowpack, and runoff peaks during the spring snowmelt period. This combination of topography and climate makes California naturally suitable for year-round hydropower production due to the sustaining summer baseflow supplied by snowmelt.

California has a deregulated electricity market, which allows for the entrance of competitors to buy and sell electricity based on the hourly-variable electricity market demand, consisting of two major morning and evening peak demands on top of the baseload (Borenstein et al., 1995, Aghajanzadeh and Therkelsen, 2019). The wholesale electricity market is comprised of distinct day-ahead and real-time markets in which the former one schedules the electricity production for the next day while the latter one is a spot market used to meet the last few increments of demand not covered in the former markets (CAISO 2016). Besides these two markets, ancillary services are to help maintain grid stability and reliability by having hydropower plants generate electricity when unexpected events occur (CAISO 2004). Hydropower is one of the important energy sources that can both undertake base load, peak load electricity generation and ancillary services (Key et al. 2012). In 2019, hydroelectric power plants accounted for 19 percent of the total in-state electricity generation in California based on the record of the California Energy Commission (CEC 2020).

A database of California hydropower plants was initially used to pair power facilities with gauging stations by locations (CEC, 2018). All the available flow records (15-minute and hourly) were obtained from the U.S. Geological Survey (USGS, 2018) and through the California Data Exchange Center (CDEC, 2018) using two R packages ("dataRetrieval" and "CDECRetrieve"). For sites whose flow records were unavailable online, public data requests were made to local managers, though not all requests were answered. Using these approaches a total of 128 records were obtained.

2.2 Data analysis framework

This study had two objectives. The first objective (OBJ 1) was to automate hydropeaking events detection and feature extraction to enable data mining in a high temporal and spatial scale. The second objective (OBJ 2) was to explore the diversity of hydropeaking flow regimes in California with outputs from OBJ 1. A data analysis framework was developed to process hydropeaking flow and identify patterns of hydropeaking flow regimes (Fig. 1). To fulfill OBJ 1, Hydropeaking Event Detection Algorithm (HEDA) was developed (Details in section 2.4). To yield better performance, flow records were split into climatic dry and wet seasons because precipitation or snowmelt can disturb hydropeaking signals. Then, outputs of HEDA were used to identify gauging stations recording hydropeaking flow and extract hydrologic metrics. To fulfill OBJ 2, two types of clustering analyses, hierarchical and fuzzy clustering, were conducted to explore data structure with seven independent hydrologic metrics of dry season dataset. Clustering analyses were heuristically determined with a combination of statistical interpretation, the examination of hydrographs, and documentation mining. Five major outcomes (highlighted in grey rectangular in Fig 2) were investigated and are discussed herein.

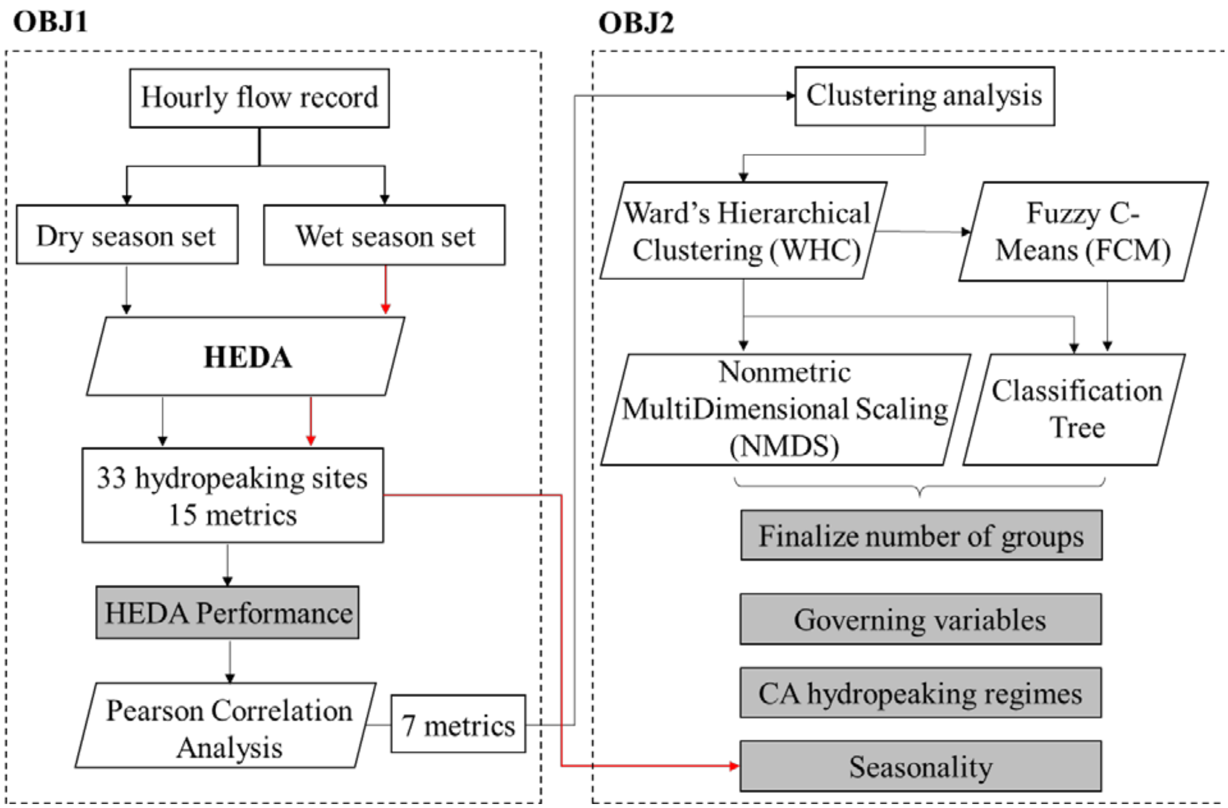

Figure 1. Data analysis frame of revealing the diversity of hydropeaking flow regimes.

2.3 Hydrologic variables

Five key dimensions of a hydrologic regime defined by Poff et al. (1997) were applied to analyze hydropeaking flow regimes. Fifteen ecologically meaningful flow metrics were then selected to represent these five dimensions (Baker et al. 2004, Meile et al. 2011, Bieri 2012, Bevelhimer et al. 2015) (Table 1). Each hydropeaking event is divided into base, rising, peak, and falling processes (Fig. 2). For each event, base flow is the minimum flow while peak flow is the maximum flow of a hydropeaking event. Rising and falling processes are the transition between base and peak flow. When two increases above the threshold magnitude are interspersed with a short period of no change, these two increases are counted as two rising processes (highlighted in dark grey in Fig. 2). Daily and annual frequency of hydropeaking are the sum of rise and fall process per day, and the number of days with hydropeaking per season/year respectively. One rise-fall cycle forms one hydropeaking event (highlighted in light grey in Fig. 2) Timing is the date/time at which hydropeaking happens. Duration is the time length of rise/fall (D_{RC}) and peak (PK_{rtn}). Rate of change (RC) is the flow variation per unit time and Richards-Baker (RB) Index describes the normalized flow variation per unit time, where the impact of river size is eliminated by normalizing with Q_{ave}.

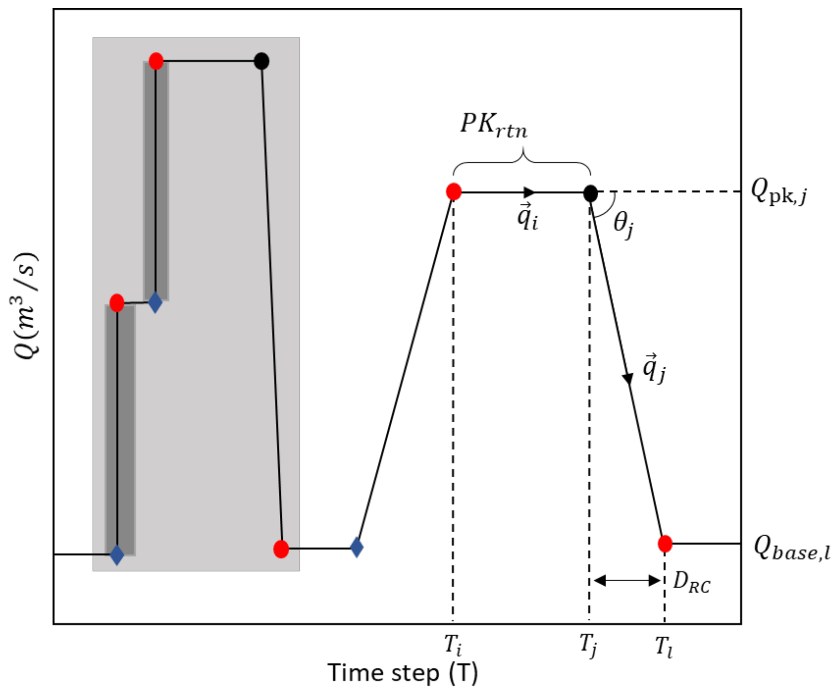

Figure 2. Events' definition and relevant values to calculate flow fluctuation parameters. Two hydropeaking events occur in the hydrograph. Vector angle (θ_j) is defined as the angle between two flow vectors ($\vec{q_i}, \vec{q_j}$).

Table 1. Hydrologic metrics derived from HEDA used in classification. Illustration was provided in figure 2.

Variable	Metric	Metric Name	Symbol	Unit
Magnitude	$\frac{Q_{pk,i}}{Q_{ave}}$	Peaking discharge	Q_{peak}	-
	$\frac{Q_{base,l}}{Q_{ave}}$	Base flow	Q_{base}	-
	$\frac{\lvert Q_{pk,j} - Q_{base,l}\rvert}{Q_{ave}}$	Standardized amplitude	$*St_{rg}$	-
Frequency	Total number of rise and fall per day. One rise-fall cycle is one hydropeaking event.	Daily peaking number	PK_{no}	-
	Number of days has hydropeaking divided by the total number of days	Annual frequency	PK_{ratio}	-
Timing	Weighted value of time (1-24) hydropeaking happens per day.	Timing	$**T_{max}$	hr
Duration	$\lvert T_i - T_j\rvert$	Retention of peak	PK_{rtn}	hr
	$\lvert T_j - T_l\rvert$	Duration of rise/fall	$*D_{RC}$	hr
Rate of change	$\frac{\lvert Q_{pk,j} - Q_{base,l}\rvert}{[\lvert T_j - T_l\rvert Q_{ave}]}$	Flashness	**RB Index*	hr^{-1}
	$\frac{\lvert Q_{pk,j} - Q_{base,l}\rvert}{\lvert T_j - T_l\rvert}$	Rate of Change	**RC*	$(m^3/s)/hr$

$*D_{RC}$, RB Index, St_{rg} and RC are split into rise and fall processes and each process is calculated separately.

$**$The weighted average value of T_{max} instead of the median value was used because of the multi-modal distribution due to morning and evening peaks, which led median value fails to represent the most frequent value of timing. Therefore, T_{max} refers to the pattern of timing rather than the time hydropeaking happens. Q_{ave} is the average discharge of the whole period of each site.

2.4 Hydropeaking Event Detection Algorithm

To fulfill OBJ 1, a new algorithm, Hydropeaking Event Detection Algorithm (HEDA), was developed in R (R Core Team, 2020) to automate feature extraction of high-resolution hydropeaking flow with limited subjective decisions. HEDA consists of three modules: Data Preparation, Vector Angle, and Clean Noise (Fig. 3). The first module, Data Preparation, starts with hourly flow records (15-minute records were converted to hourly records by taking the mean flow within the same hour) of the interest period (e.g., post-dam period). The flow record of each site is then split into dry (June-September) and wet (October-May) season datasets to optimize the performance of HEDA as hydropeaking tends to occur more frequently in the dry season while precipitation and snowmelt in other seasons can disturb the hydropeaking signals. Data smoothing strategies such as Gaussian filtering or locally estimated smoothing were not applied as these strategies (1) are unable to quickly process a large amount of data; (2) potentially mark peaking events as noise; and (3) degrade or destroy the peaking pattern (SI II). Instead, the flow record was smoothed with two steps. First, based on observation, intensive small fluctuations always occur at base and peaking discharge, thus flow records were truncated by 10th and 90th percentile of discharge during the whole period(SI II). Second, flow variations ($\Delta q_i = Q_{i+1} - Q_i$) smaller than threshold X were assigned zero to avoid mischaracterizing small fluctuations as peaks due to measurement errors. Threshold X consists of a global (γ) and local static ($\alpha_1 * Q_{ave}$) threshold (Eq.1). The global threshold (γ) acted as a consistent standard to all sites. Threshold values of γ was initialized based on the minimum rise/fall rate found in the literature (2.8 m^3/s/hr) and finalized to be γ = 1.1 m^3/s. The local static threshold ($\alpha_1 * Q_{ave}$) was a consistent standard to one site. The α_1 was assigned 0.03 by evaluating the range of Q_{ave} at 33 sites and the relative difference between all the thresholds ($T3_t$) used in this study (SI II).

$$X = \max(\gamma,\ \alpha_1 * Q_{ave}) \tag{1}$$

The second module, Vector Angle, involves the identification of change points (Fig. 3). Among the flow record, consecutive data points (T_n,Q_n) and (T_{n+1}, Q_{n+1}) were treated as a Euclidean Vector $\overrightarrow{q_n}$ ($\Delta t_n,\ \Delta q_n$), a quantity that has a magnitude and a direction. The magnitude of a vector is the distance between the two data point ($|\overrightarrow{q_n}| = \sqrt{(\Delta t_n)^2 + (\Delta q_n)^2}$ while direction is from its tail (T_n,Q_n) to its head (T_{n+1}, Q_{n+1}) (Fig. 2). The vector angle (θ_{n+1}) between two continuous vectors ($\overrightarrow{q_n}, \overrightarrow{q_{n+1}}$) was used to identify change points instead of the first derivative of $q(t)$ to exclude change points outside the range of the designated rise/fall rate ($\tan\theta = \Delta q_n / \Delta t_n$) (Eq.2). The threshold value of θ was tested from 30° to 70° and finalized as 70°. The degree 70° was set based on the threshold of the mitigation standard of hydropeaking rise/fall rate (2.8 m3/s/hr) used in the American river (SI II) (Young et al. 2011). After $q(t)$ with $\theta > 60°$ were identified, change points were grouped into four categories based on the symbol of Δq_{n+1} (+, 0, -) which separated hydropeaking processes into four groups (points 1-4 in Fig. 3). Points 1 and 4 are always followed by a rising discharge while point 3 is followed by a falling discharge. Point 2 indicates the start of either a peak or base flow discharge. The sequence of point 2 followed by point 4 (base-flow pair) indicates base flow while the combination of point 2 and 3 (peak pair) indicates a peak discharge.

$$\theta_{n+1} = \cos^{-1}({\Delta t_n}^2 * {\Delta t_{n+1}}^2 + {\Delta q_n}^2 * {\Delta q_{n+1}}^2) / \sqrt{\Delta q_n * {\Delta t_n}^2 + \Delta q_{n+1} * {\Delta t_{n+1}}^2} \quad (2)$$

In the Clean Noise module, three layers of correction (position, repetition and difference) clean change points identified incorrectly. In the position layer, change points are excluded if they occur in the wrong position. For example, both point 3 and the peak pair represent the peaking discharge whose value (position) should be close to the daily maximum discharge. If the peaking discharge is close to the daily minimum discharge, change points are removed since they are in the wrong positions. The second layer, Repetition, cleans repeated points generated in the first layer. Before getting to the third layer, the first and second layers need to repeat to make sure change points that violated the former two rules are removed. The last layer, Difference, evaluates whether Δq_i is large enough to be identified as a peaking event based on a daily amplitude threshold described below.

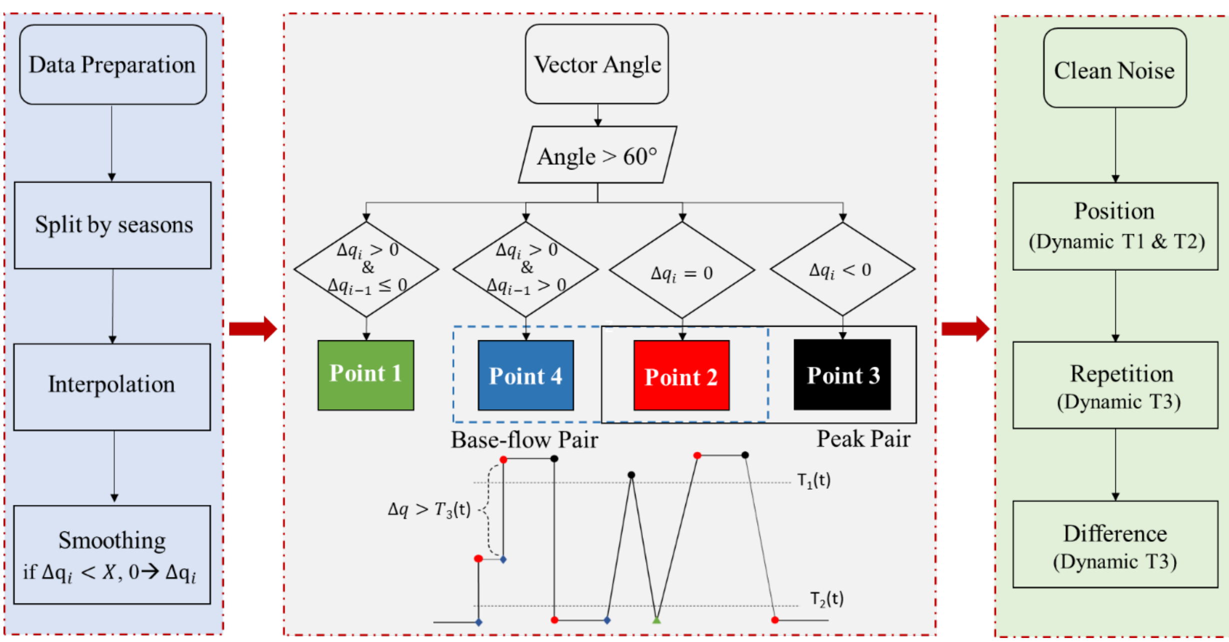

Figure 3. Schematic diagram showing the sequential steps of the HEDA.

Within the three layers, three thresholds were used, $T1(\mathrm{t})$, $T2(\mathrm{t})$, and $T3(\mathrm{t})$ (Eq.3-5 and Fig. 3). In the position layer, two dynamic thresholds ($T1(\mathrm{t})$ and $T2(\mathrm{t})$) that were updated daily were used for each river to identify the relatively high and low discharge. The threshold value of high discharge was defined as the difference between maximum daily flow ($Q_{max}(\mathrm{t})$) and 30% (α_2) of the daily maximum amplitude ($Q_{max}(\mathrm{t}) - Q_{min}(t)$) while that for low discharge was defined as the sum of daily minimum flow ($Q_{min}(t)$) and 30% (α_2) of the daily maximum amplitude. In the repetition and difference layers, $T3(\mathrm{t})$ was used as the standard to evaluate whether flow variation can be counted as a rise/fall process. $T3(\mathrm{t})$ consists of a local static threshold ($\alpha_3 * Q_{ave}$) and a dynamic threshold ($\alpha_4 * (Q_{max}(\mathrm{t}) - Q_{min}(t))$) that were updated daily for each river to reflect the evolvement evolution of climate, seasonality, and river size flow, all of which that are highly related to hydropower operation. To decide what fraction of Q_{ave} to be used, tests were run within a reference range (30%-100%) obtained from literature with both Q_{ave} and amplitude available (Zimmerman et al. 2010, Hauer et al. 2012, Capra et al. 2017). Finally, 70% of Q_{ave} ($\alpha_3 = 0.7$) was selected as the threshold value because outputs of HEDA didn't change beyond this fraction. To identify different intensities of rise/fall process of each site, 50% of the daily maximum amplitude was used (SI II).

$$T1(\mathrm{t}) = Q_{max}(\mathrm{t}) - \alpha_2 * (Q_{max}(\mathrm{t}) - Q_{min}(t)) \tag{3}$$

$$T2(\mathrm{t}) = Q_{min}(\mathrm{t}) + \alpha_2 * (Q_{max}(\mathrm{t}) - Q_{min}(t)) \tag{4}$$

$$T3(\mathrm{t}) = \max\big(\alpha_3 * Q_{ave} \, , \, \alpha_4 * (Q_{max}(\mathrm{t}) - Q_{min}(t))\big) \tag{5}$$

The performance of HEDA was assessed with visual examination, with 500 change points of each hydropeaking site plotted and visually checked. The error rate of HEDA was calculated by dividing the number of wrongly identified change points by 500.

2.5 Hydropeaking clustering

To fulfill OBJ2, outputs from HEDA of dry season dataset were analyzed with correlation analysis to select independent metrics for clustering analysis to explore the underlying diversity of hydropeaking flow regimes among the 33 sites. First, values of 15 metrics were transformed to values between 0 and 1 by min-max normalization (Eq. 6) to remove scaling impact. A correlation matrix of fifteen flow metrics was created to identify and remove highly correlated metrics (SI I). Second, two types of clustering methods, hierarchical and fuzzy clustering, were used to explore the data structure from different perspectives. In the beginning, a hierarchical clustering analysis using Ward’s algorithm (Ward’s hierarchical clustering; WHC) (Ward, 1963) was used to make a preliminary assessment of hydropeaking patterns without any preconceived assumptions. The WHC started with the maximum cluster number (33 in this study), then reduced the number of clusters by merging them at the node with minimum merging cost, i.e. the least total within-cluster variance, from bottom to top. Then, Fuzzy c-means (FCM) clustering built on the WHC result was used to not only examine the clustering structure with the partitional-clustering algorithm but also the degree of membership (Bezdek 1973, 2013). Instead of assigning one site to one class each time, FCM assigned each site a cluster membership score, where being closer to the cluster center means a higher score. This provided more robust clustering against noise and outliers because low scoring sites have a reduced impact on the position of the cluster center (Kantardzic 2011). Also, presuming a soft boundary between clusters is more aligned with real-world hydropower operation since its underlying driving force is to maximize profit under constrained factors; thus, a powerhouse might use more than one operational mode.

$$Y'_i = \frac{Y_i - Y_{min}}{Y_{max} - Y_{min}} \quad (6)$$

The relative roles of hydropeaking metrics forming the data structure were analyzed next. Nonmetric multidimensional scaling (NMDS) (Clarke, 1993) was performed to visualize the hidden structure of the multivariate dataset in a reduced dimension (from seven to three dimensions). Principle component analysis was then built on NMDS to evaluate the relative significance of the seven metrics on each axis. Box-and-whisker plotting was applied to illustrate relative differences in hydrologic metrics within and across the identified hydropeaking patterns. Finally, a classification and regression tree (CART) (Breiman et al., 1984, De'ath and Fabricius, 2000) was used to identify the most explanatory hydrologic metrics in distinguishing hydropeaking patterns and their threshold values. The classification tree yielded a binary decision tree based on the proportion of presences and absences in the clusters. The splitting criterion was to maximize the homogeneity of the cluster and is defined by the Gini index which measures the degree or probability of a particular variable being wrongly classified when it is randomly chosen. At each node, the selected feature/metric with the lowest Gini index was used to further split the tree. Euclidean distance was chosen as the distance measure. Ten-fold cross-validation was used to select tree size with the highest prediction accuracy.

Clustering validation was heuristically determined based on a combination of statistical analysis interpretation, the examination of hydrograph and documentation mining. First, potential numbers of clusters were identified based on the structure of the dendrogram and the Hartigan index (Hartigan 1975). Meanwhile, NMDS was used to visualize how potential clusters distinguish sites in a reduced dimension. The goal is to have clusters well separated from each other with the least overlapping areas. Second, site membership in clusters was analyzed and only those with a value > 50% were kept. Third, box-and-whisker plots and classification trees were also used to examine the performance of clustering. For reliable clustering, it is expected that metrics display a certain degree of difference between clusters, and classifiers trained by identified clusters can perform prediction reliably (cross-validation accuracy). Besides all the statistical interpretation, physical interpretation of the clusters was also conducted by checking hydrograph and historical documentation of hydropower facilities. The goal of this heuristic refinement was not to make large adjustments to the purely statistical classification but to ensure that it was capturing real-world differences.

3 Results

3.1 Identification of hydropeaking sites

Before attempting to use HEDA to identify hydropeaking sites, the performance of HEDA was assessed (Fig. 5) by applying it to sites where operation modes were known (30 non-hydropeaking and 10 hydropeaking sites). HEDA worked effectively at distinguishing the non-hydropeaking flow from the hydropeaking flow. Compared with the hydropeaking flow, half of the non-hydropeaking flow sites obtained "NA" output (no value) for all metrics and the other half featured low PK_{ratio} (<5%) and PK_{No} (<0.9). Hydropeaking flow was defined as having high PK_{ratio} (10%-95%) and PK_{No} (>=1). Then, these criteria for PK_{ratio} and PK_{No} were employed as standards to identify sites using all 128 flow records. Sites that met only one of the two standards (PK_{ratio} and PK_{No}) were double-checked with hydrographs and documentation about site operations.

Consequently, 33 sites (site information in SI I) with a length of flow records at least five years were identified as hydropeaking sites and used for the following analyses (Fig. 4).

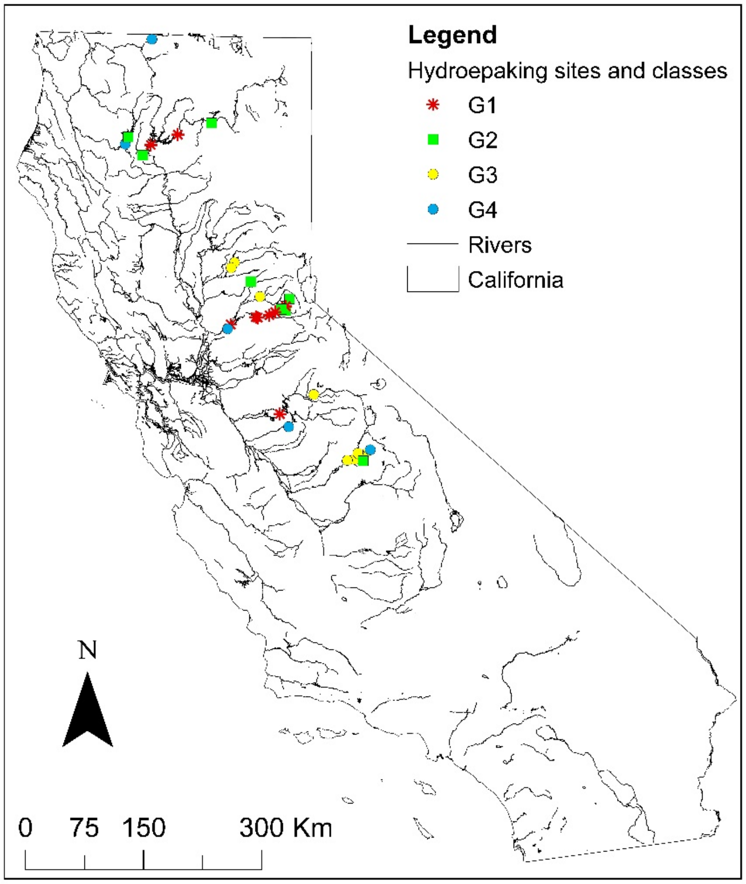

Figure 4. Map of hydropeaking sites identified by HEDA and classes identified by FCM, California, USA. An interactive map is available: https://ninalty.github.io/HPK_InteractiveMap/HPK_CA_InteractiveMap.html

Among the 33 hydropeaking sites, the average error rate of HEDA was 1% among sites with minimum and maximum values of 0% (six sites) and 2.8% (two sites), respectively. The incorrect change points were mainly caused by noisy segments of flow records from local agencies that did not perform sufficient quality assurance and quality control, yielding data that were too noisy even for manual identification (Fig. 5A). As for other flow records, relatively small peaking events can be neglected by HEDA when a mix of small and large peaking events occurred on the same day. The large peaking discharge can make the upper bound of peaking ($T1(\mathrm{t})$) too high for small peaking events to be detected. For example, in FOL site, the large peaking discharge is around 142 m^3/s while the small peaking discharge is around 71 m^3/s on the same day. Because of the large relative difference between hydropeaking events within that day, HEDA can only keep the large hydropeaking events but overlook the small ones (Fig. 5B).

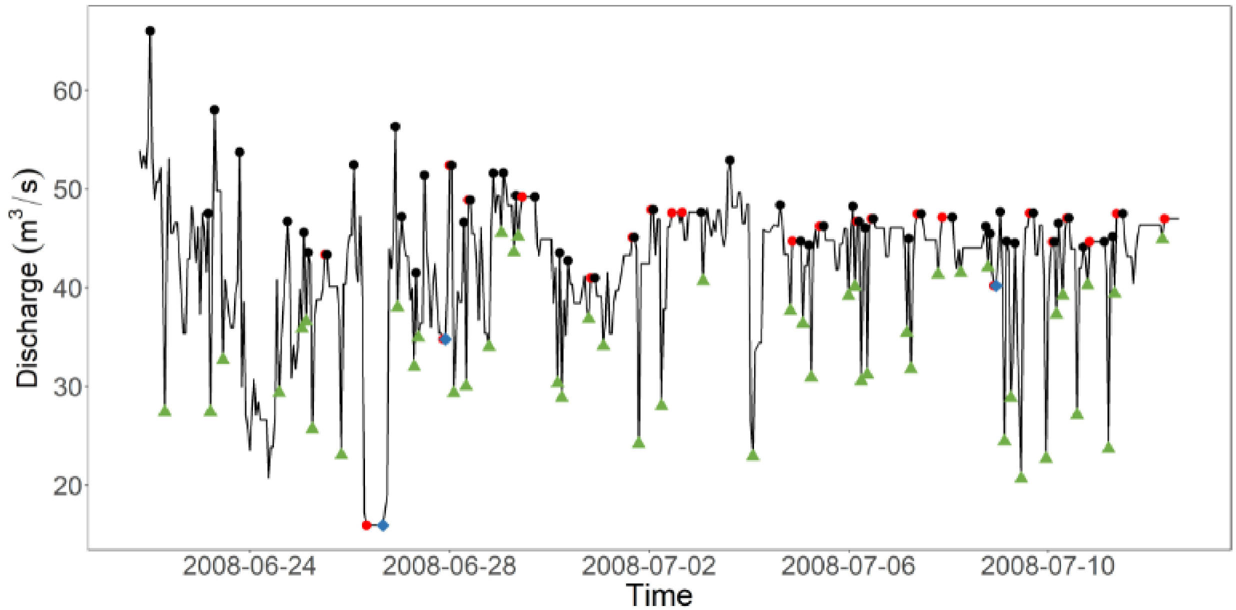

A

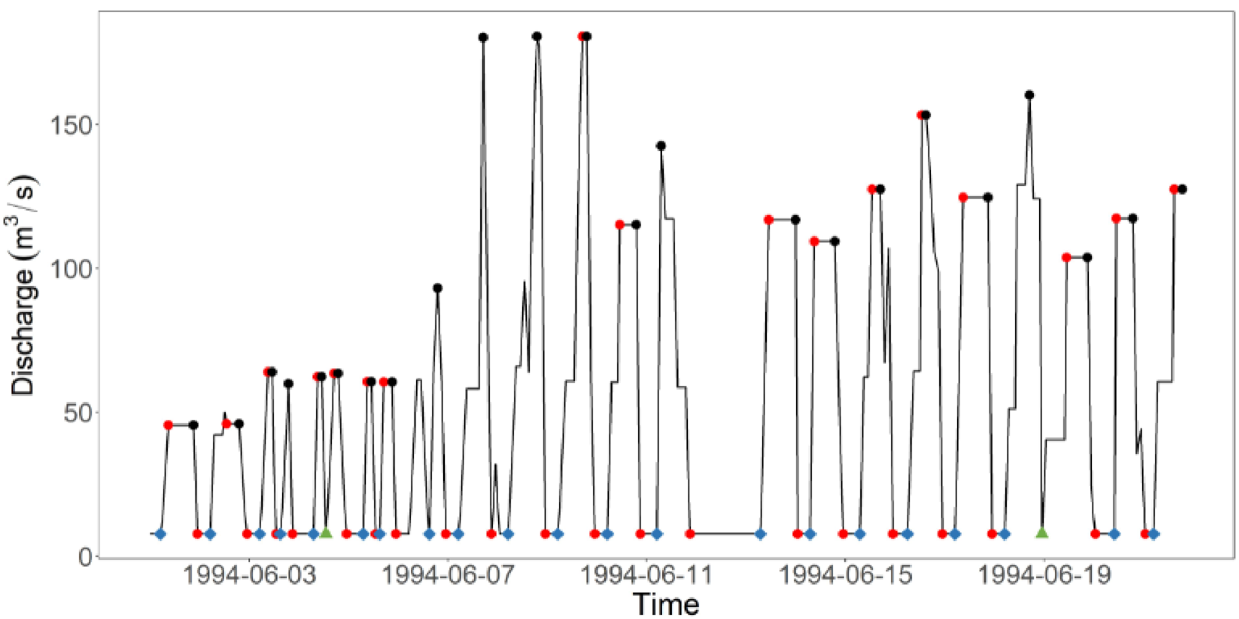

B

Figure 5. Hydrographs with 500 change points identified by HEDA in the dry season. A is streamflow below Big Creek Power House #3 recorded by gauge 11241800. B is streamflow below Folsom Lake outflow recorded by gauge FOL.

3.2 Diversity of hydropeaking flow regimes

Outputs of HEDA (median values of 15 flow metrics) were further analyzed to reveal the diversity of hydropeaking flow regimes. Seven metrics were selected and regarded as uncorrelated (≤ 0.6) (SI II). Even though PK_{ratio} is moderately related (0.69) to D_{RC} among the seven metrics, PK_{ratio} was still selected because it can provide the number of days that hydropeaking occurs during a certain period, such as summer in this case. As for the other six metrics, the correlation coefficients between them were all below 0.6 and assumed to be weakly related. With a normalized subset of hydrologic metrics meeting statistical independence, WHC was first applied to illustrate the nested data structure of the 33 sites (Fig. 6). The first split occurred at a distance of 2.8, distinguishing two clusters: one giant cluster and one small cluster – group four (G4). Subsequently, the tree split within the giant cluster and formed four big branches: group three (G2), group two (G3) and group one (G1) in sequence. All the subtrees continued to grow under each of the four branches. However, the internal clustering Hartigan index suggested that cutting the dendrogram into four groups was the optimal option driven by strong breaks in D_{RC}, PK_{No} and PK_{ratio}. This conformed with preliminary analyses of data structure in the reduced dimensions (NMDS) and tree structure of the clustering dendrogram (Fig. 7). To have four clusters, the tree was cut at a distance of 2, and 11 sites were clustered to G1, eight sites as G2, nine sites as G3 and four sites as G4.

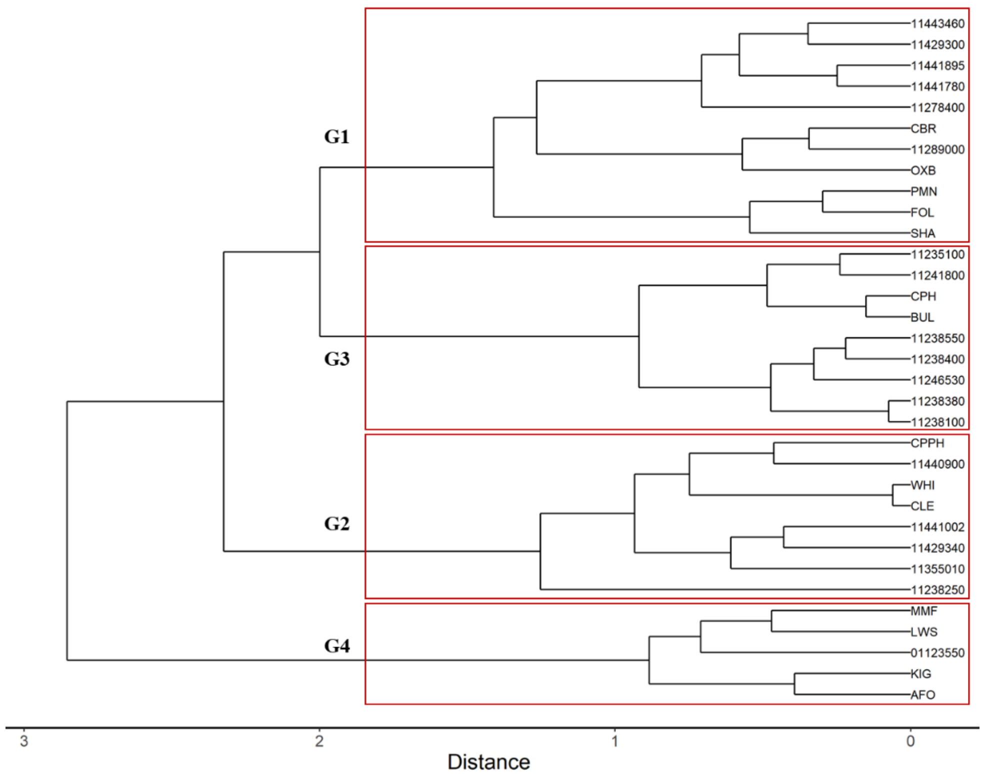

Figure 6. The hierarchical cluster diagram shows similarity/dissimilarity among 33 sites. Sites are indicated by either their USGS ID number or the CDEC 3-character ID.

To further evaluate clustering validity or uncertainty, FCM clustering was applied to assess the strength of WHC by knowing the membership value of each site in the identified groups. The fuzzification parameter (m) is a weighting parameter controlling the degree of fuzziness in the process of clustering. When m=1, the partitioning is 'hard' (probability of members to the designated cluster is one), as m increases the membership assignments of the clustering become fuzzier (members have evenly distributed probability in all clusters). Even though no theoretical or computational evidence distinguishes an optimal m, for most data sets, $1.25 \leq m \leq 3$ gives good results (Bezdek et al. 1984, Güler and Thyne. 2004, Ross 2005). Based on trials and sensitivity testing in this study, it appeared that m = 1.3 resulted in clustering that was neither too fuzzy nor too hard. From the membership matrix (Table 2), sites were assigned to the cluster of membership value > 0.5. Compared with WHC, assigning the same cluster number to FCM generated a similar clustering structure with only two sites clustered to different groups. Site 11278400 and OXB were moved from G1 to G3 and G2 by FCM. Site OXB had a weak membership in all the groups.

Table 2. FCM Membership Matrix of hydropeaking patterns. Bold numbers indicate group membership selected.

Sites	Group	Membership value			
		G1	G2	G3	G4
11278400	G3	0.40	0.04	0.54	0.01
11289000	G1	0.50	0.39	0.10	0.01
11355010	G2	0.10	0.86	0.03	0.00
11429300	G1	0.96	0.02	0.03	0.00
11429340	G2	0.04	0.94	0.02	0.00
11440900	G2	0.00	0.99	0.00	0.00
11441002	G2	0.06	0.94	0.00	0.00
11441780	G1	0.98	0.02	0.01	0.00
11441895	G1	1.00	0.00	0.00	0.00
11443460	G1	0.99	0.00	0.00	0.00
11238100	G3	0.00	0.00	1.00	0.00
11238380	G3	0.00	0.00	0.99	0.00
11238400	G3	0.00	0.00	1.00	0.00
11241800	G3	0.00	0.00	1.00	0.00
11246530	G3	0.00	0.00	1.00	0.00
11238550	G3	0.00	0.00	1.00	0.00
11235100	G3	0.00	0.00	1.00	0.00
01123550	G4	0.00	0.03	0.02	0.95
11238250	G2	0.16	0.74	0.08	0.02
AFO	G4	0.00	0.00	0.00	1.00
BUL	G3	0.03	0.00	0.97	0.00
CBR	G1	0.94	0.01	0.05	0.00
CLE	G2	0.01	0.99	0.00	0.00
CPH	G3	0.09	0.01	0.90	0.00
CPPH	G2	0.00	1.00	0.00	0.00
FOL	G1	0.94	0.05	0.01	0.00
KIG	G4	0.00	0.00	0.00	1.00
LWS	G4	0.00	0.00	0.00	1.00
MMF	G4	0.00	0.00	0.00	1.00
OXB	G2	0.17	0.38	0.32	0.13
PMN	G1	0.98	0.00	0.01	0.00
SHA	G1	0.92	0.04	0.03	0.01
WHI	G2	0.01	0.99	0.00	0.00

3.3 Clustering validity and relative significance of hydrologic metrics

Clustering validation was heuristically evaluated by exploring the data structure in a reduced dimension and analyzing the relative significance of the hydrologic metrics of each group. The three-dimensional NMDS ordination reached a stress value of 0.085 with a non-metric coefficient of determination of 0.99 between observed dissimilarity and ordination distance (Fig. 7) which both indicate a good ordination with little risk of drawing false inferences (McCune et al. 2002). In the reduced dimensionality, along the first axis, five sites that belonged to G4 were well apart from the majority on the right side. Sites gathered on the right spread widely along the second axis and had a small overlapping area between G1 and G3. The three principal component axes (PCAs) resulting from the NMDS ordination explained 74% of the variance in the data with loadings of 0.65 for PK_{ratio}, -0.78 for PK_{rtn} and -0.65 for PK_{no} for PCA-1, PCA-2 and PCA-3 respectively. Besides PK_{rtn}, D_{RC} ranked the second highest (0.60) loadings for PCA-3. These analyses led to the conclusion that PK_{ratio} was the principle metric that distinguished G4 from the other three groups while PK_{rtn}, PK_{no} and D_{RC} together explained the separation of G1, G2 and G3.

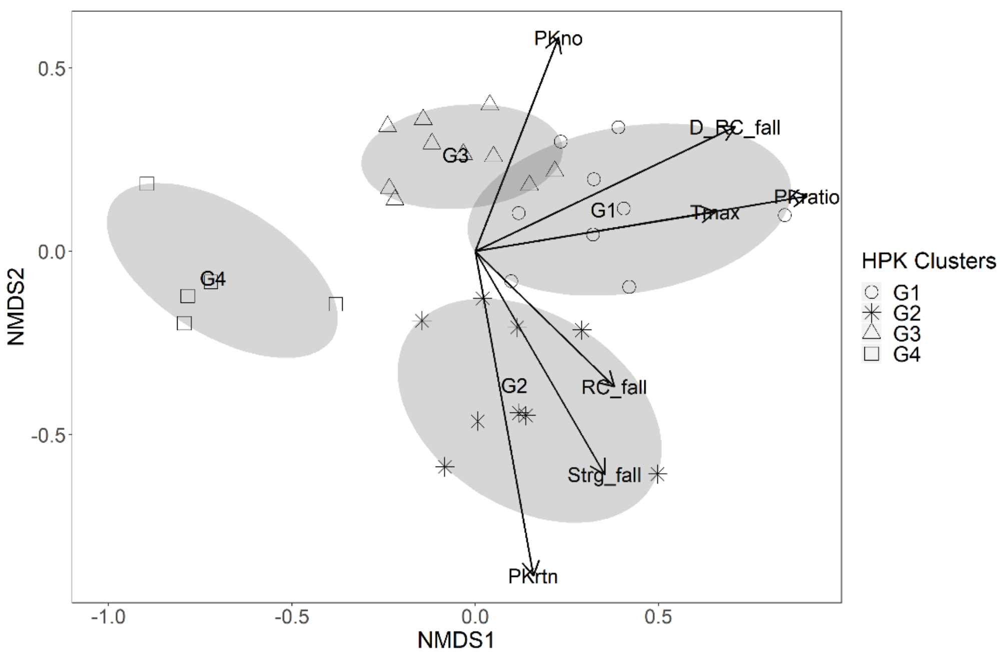

Figure 7. Results from non-metric multidimensional scaling.

Classification tree and box-and-whisker plots were used to identify the most explanatory hydrologic metrics distinguishing hydropeaking patterns and their threshold values. These provided potential ranges of metric values expected for each hydropeaking pattern. The classification tree model built on WHC determined three principle metrics and the relative strength to be as follows: PK_{no} (2.6), PK_{ratio} (46%) and PK_{rtn}(4.5) (Fig. 8). The classification tree model built on FCM determined three principle metrics and their relative strength to be as follows: PK_{no} (2.6), D_{RC} (3.5), and PK_{ratio} (46%). The classification tree built on WHC and FCM both correctly classified 94% of the sites. Ten-fold cross-validation of the prediction was 79% (WHC) and 82% (FCM). Box-and-whisker plots illustrated relative differences in hydrologic metrics within and across the four identified hydropeaking groups (Fig. 9). G1 had the highest D_{RC} and PK_{ratio} which implied G1 features a relatively slow rise/fall process and frequent peaking operations across a year. G2 had the highest PK_{rtn}, RC, and St_{rg} implying that this group has a long-lasting peaking status, with a rapid fluctuation with large variations in magnitude. G3 stood out from other groups as having the highest PK_{no} but relatively low values of other metrics compared with the former two groups. G4 has the fewest hydropeaking features, with low values of all the hydrologic metrics. G1 and G2 have similar values of T_{max} while G4 has the lowest value of T_{max} and G3 ranked between them.

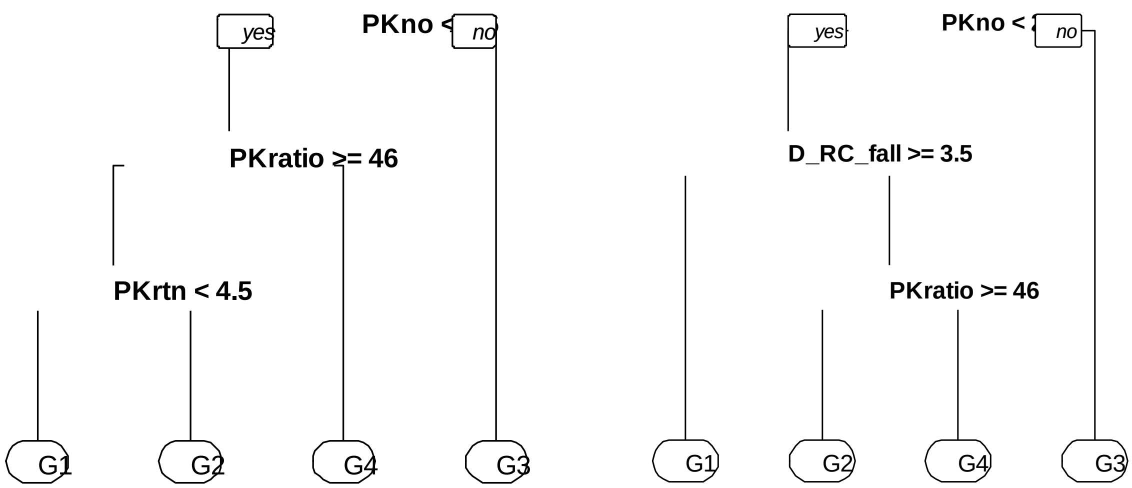

(A) (B)

Figure 8. CART classification trees indicating primary metrics and their threshold values of distinguishing hydropeaking groups trained by WHC (A) and FCM (B).

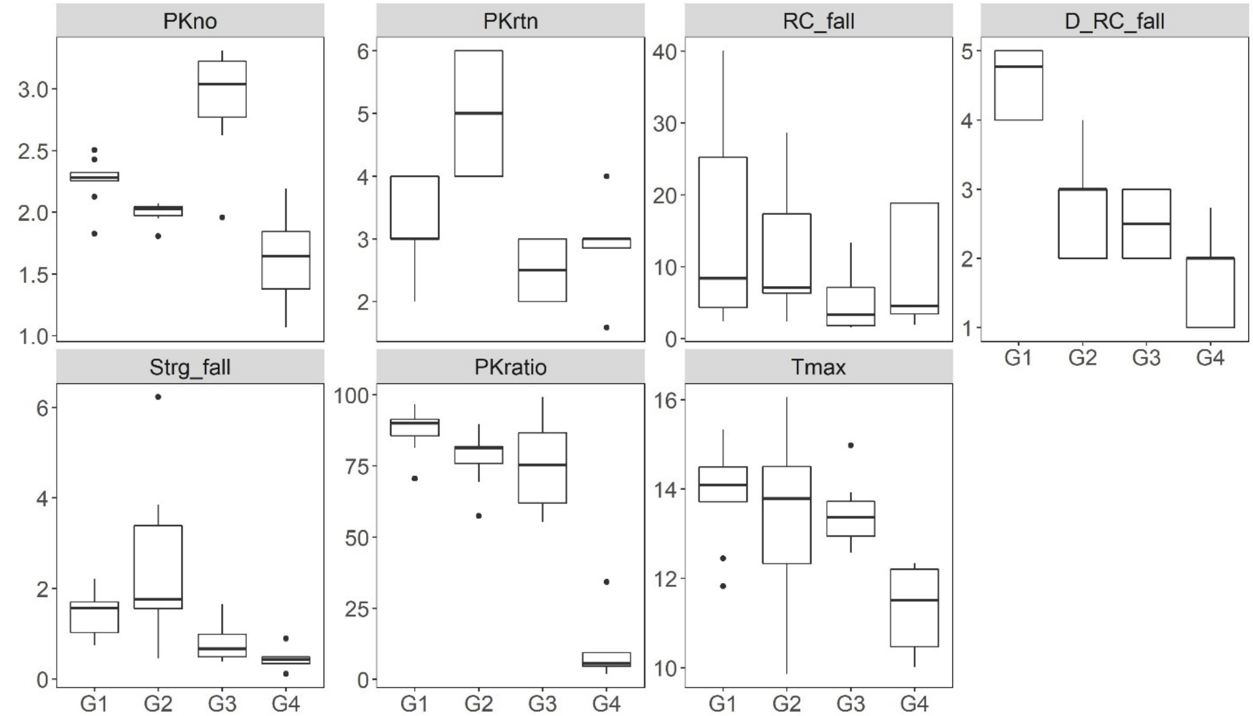

Figure 9. Box-and-whisker plot of normalized hydrologic metrics used in the FCM clustering analysis.

4 Discussion

4.1 HEDA performance

Instead of using the first derivative of discharge with time, treating consecutive points in a flow record as a Euclidean vector and detecting change points with vector angle and magnitude boosted the computational efficiency by avoiding over-detecting change points. In addition, the application of static and dynamic thresholds automatically adjusts the threshold over time and across sites. Thus, it requires less subjective input and iterative adjustment. The only subjective decisions that have been made are the four weighting coefficients α_1, α_2, α_3 and α_4. Their values were assigned based on the overall performance and reference range found in the literature, but they are open to user adjustments. All these features make HEDA stand out from other approaches for its capability of distinguishing sites with and without hydropeaking and automating the feature extraction of hydropeaking flows.

Even though HEDA initially was not developed to distinguish hydropeaking flow from non-hydropeaking flow, it successfully distinguished the two types of flow with PK_{ratio} and PK_{No}. This is a very useful function because manually pairing the location of gauges to powerhouses is extremely time-consuming. Besides known hydropeaking sites, HEDA could identify hydropeaking sites by starting with flow records instead of with documentation – which is useful in regions of the world where getting this documentation can be quite difficult or in places where actual operations deviate from stated ones. With HEDA, users can finish this process within ten minutes by importing all the sub-daily flow record of a site into HEDA. Furthermore, HEDA successfully captured major hydropeaking events and filtered noises through the whole study period (five to thirty years) of 33 sites with a low error rate (Fig. 5), thus enabling the extraction of hydrologic features automatically. Automating feature extraction of sub-daily flow on a large spatial scale opens infinite possibilities for scientific analysis, such as applications for a high-frequency sampling of many other types of flow alterations and the development of flow-ecology relationship.

4.2 Variables governing hydropeaking classification

NMDS and two types of clustering analyses were applied to explore the diversity of hydropeaking flow regimes. Together they delineated 33 hydropeaking sites into four distinct groups, providing meaningful information about differences in hydropeaking regimes in California. The finalized classification built on WHC and FCM were examined by classification trees with ten-fold cross-validation. Even though both WHC and FCM generated similar clustering structures, the classification tree built on FCM had a higher accuracy of prediction than that on WHC. As for variables that govern the classification of hydropeaking, frequency and duration of peaking events were identified by classification trees. Specifically, PK_{no}, PK_{ratio}, and PK_{rtn} distinguished the four classes G1-G4 in the classification tree built on WHC while PK_{no}, D_{RC} and PK_{ratio} distinguished G3, G4, G2 and G1 in the classification tree built on FCM. In both trees, daily number of peaking events (PK_{no}) is the principal metric distinguished G3 from the other three groups. The annual frequency (PK_{ratio}) was the principal metrics distinguished G4 from the other two groups. Meanwhile, the structure of classification tree built on FCM indicated that G4 also featured rise/fall process with a smaller duration. As for G1 and G2, duration of peaking and rise/fall distinguished these two groups from each other. The magnitude, rate of change and timing were not identified as principal metrics that differentiated the four groups which indicates that these features of hydropeaking events are similar among all hydropeaking sites. However, the governing variables might change in different regions.

4.3 California hydropeaking regimes

Four representative hydrographs of the identified hydropeaking groups/patterns were created for California (Fig. 10). G1 has the strongest hydropeaking regime due to high values in all metrics except the peaking retention and standardized amplitude. G2 ranks the second strongest peaking regime with long-lasting peaking retention (≥ 5 hr) and highest amplitude (two to four times mean annual discharge). Compared with G1, G2 represents a hydropeaking pattern that peaks less frequently but with a relatively longer peak each time due to the high peaking retention. These two groups describe hydropower plants with large generation capability or reservoirs which allows them to handle major hydropeaking tasks. In G3, all metrics values are smaller than those of the former two groups, but had the highest number of daily peaking events. This indicates G3 represents hydropower plants that conduct hydropeaking more frequently on a daily basis but with lower magnitude and duration. Its relatively low annual frequency of peaking might imply that this group is not responsible for the major hydropeaking source of energy in California. G4 represents the weakest hydropeaking regime. Even though its PK_{ratio} is extremely low ($\leq 41\%$), the value of PK_{No} and PK_{rtn} strongly suggests that hydropeaking regulation still exists. This is an interesting group because its weak hydropeaking features are caused either by environmental restriction or the type of powerhouse. For example, the environmental restriction has been applied to Nimbus Dam (gauge AFO) to reduce steelhead trout stranding (Young et al. 2011). Thus, the downstream flow recorded by AFO still displays the peaking pattern but with a lower magnitude, frequency, and rate of change. The Merced Falls powerhouse (gauge MMF) is a run-of-the-river facility using water downstream of an impoundment. The impoundment's release capability limits its capability of generating strong peaking flow (McManamay 2016).

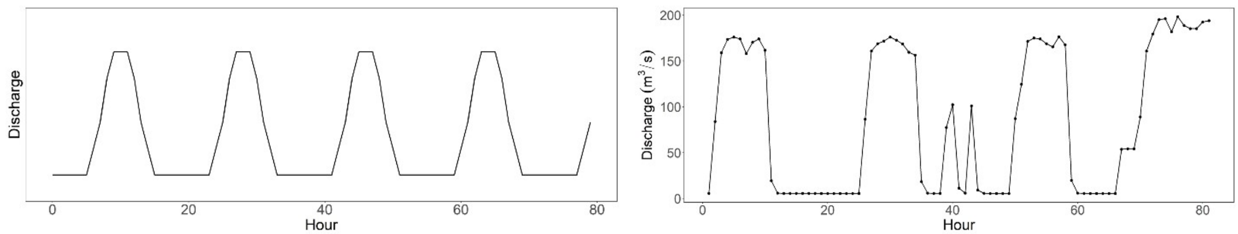

G1 Frequent hydropeaking

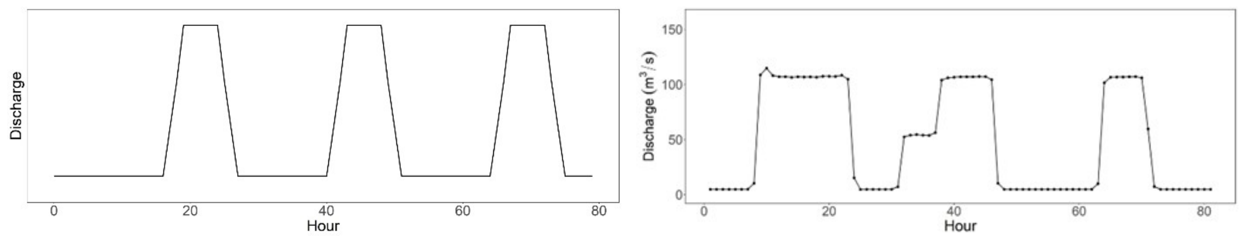

G2 Large hydropeaking

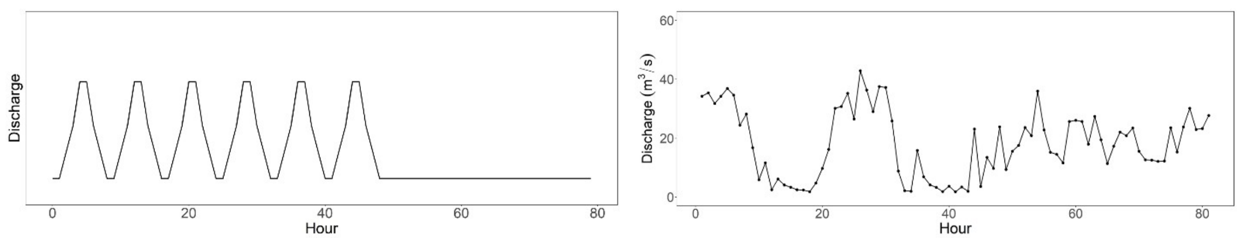

G3 Supplementary hydropeaking

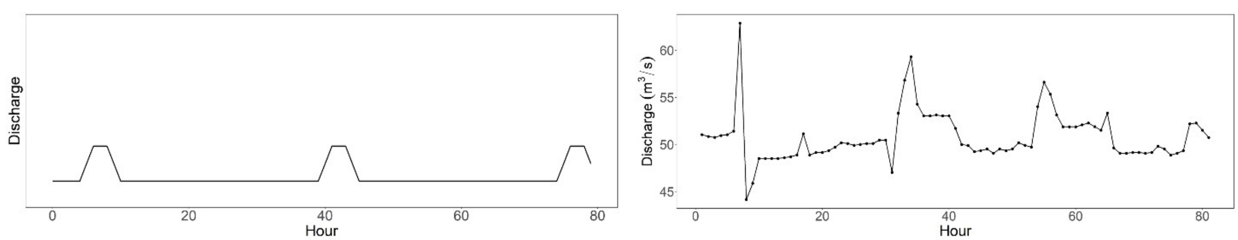

G4 Regulated hydropeaking

Figure 10. Representative hydrograph of the identified hydropeaking classes (left) and site member of each class (right; G1 gauge PMN; G2 gauge WHI; G3 gauge BUL; G4 gauge AFO). In G3 and G4, the typical morning and night timing pattern was not obvious. G3 features hydroelectricity generation mainly for ancillary services which were built for maintaining grid stability and reliability when unexpected events happened. G4 features those regulated hydropeaking flow. Flow alteration in G4 consists of hydropeaking flow and environmental flow for aquatic ecosystem and river channel. Therefore, these two factors disturbed the timing of hydropeaking in G3 and G4 respectively.

4.4 Seasonality of California hydropeaking flow regimes

The seasonality of hydropeaking was assessed in terms of the variation of hydropeaking operations between the wet and dry seasons that comprise the annual cycle of the Mediterranean climate in California. Another prominent feature of this climate is pronounced interannual precipitation variability. Thus, we also examined differences in hydropeaking between years with above- and below-normal precipitation. Representative drought and non-drought years were set to be 2014 and 2017 separately due to the availability of data (SI I). The dry season of the two representative years was selected as the reference season.

Generally, the annual frequency of hydropeaking in dry season was higher than that in wet season. The difference in annual frequency of hydropeaking between dry and wet season was over 10% in G1 (10%), G2 (13%) and G3 (17%) while was negligible (1%) in G4. These results indicated that sufficient water availability during wet season allows hydropower facilities to generate electricity constantly while hydropeaking operations are much more intensive in dry season due to the scarcity of water. In addition, the annual frequency of hydropeaking in the dry season is positively related to hydropeaking frequency in wet season indicated by the uncrossed lines of two seasons (Fig. 11). That to say, sites that tend to conduct hydropeaking frequently in dry season are more likely to have high annual frequency of hydropeaking in wet season. As for the variance of hydropeaking between different types of years, the non-drought year had a lower annual frequency of hydropeaking operation than that in drought year for all groups. And the difference between them followed the similar pattern identified in the comparison of wet and dry seasons. The annual frequency of hydropeaking in drought year was 12%, 7% and 10% higher than that in non-drought year in G1, G2 and G3 respectively. Meanwhile, the hydropeaking signals almost disappeared in G4.

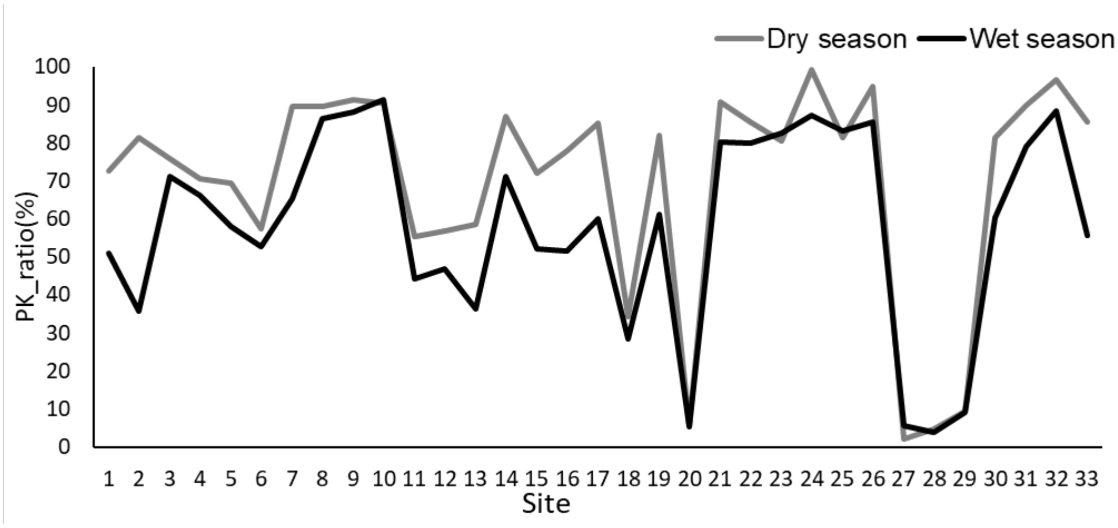

Figure 11. Annual frequency of hydropeaking during dry and wet seasons.

4.5 Uncertainty of the classification

Three types of uncertainties exist in this study: the uncertainty in knowledge about the operation of hydropower facilities, the uncertainty caused by the method, and the uncertainty associated with input data. As for operation uncertainty, because the underlying driving force of hydropower operation is to maximize profit, thus, more than one operation mode might be conducted by one powerhouse. Fuzzy classification was applied to explore the proportion of different types of hydropeaking operation modes at one site. Even though four distinct groups of hydropeaking were revealed, three sites have more than one dominant type of hydropeaking (gauge OXB, 11278400 and 1128900). For example, both gauge OXB and 11278400 had an even membership in two groups, indicating that two types of hydropeaking operation modes jointly exist. Methodological uncertainty originated from threshold values, especially the annual mean flow-based threshold (X and $T3_t$). Seasonal flow-normalization was recommended for future research to avoid bias introduced by the extreme dry/wet years. Even though thorough tests were conducted and coefficients of annual mean flow were selected due to the stable outputs of HEDA, it is possible that the generality of HEDA cannot capture some details of the hydropeaking flow regime of an individual river. Therefore, it is highly recommended to adjust these coefficients if a single river is studied (Table 1 in SI II). Input data uncertainty arose from the scarcity of sub-daily flow records, particularly for streamflow, penstock flow and reservoir outflow. Reservoir outflow and penstock flow record the most original flow regime of hydropeaking flow which can be used to infer the operation of facilities while streamflow records the degraded hydropeaking flow regime but is valuable to the study of flow-ecology relationships.

5 Conclusions

In this study, a new method (HEDA) has been developed in R statistical software to automate hydropeaking feature extraction with minimal subjective decisions, adjustments, and iterations. This allows for an analysis of hydropeaking flow at a large temporal and spatial scale. Then, hierarchical and fuzzy clustering analyses were used to explore and discover hydropeaking patterns in California, using seven ecologically relevant hydrologic metrics computed by HEDA. Four hydropeaking flow regimes have been identified: Frequent (G1), Large (G2), Supplementary (G3), and Regulated hydropeaking flow regimes (G4). G1, frequent hydropeaking, is characterized by long rise/fall processes of an individual peaking event (≥ 3.5 hr) but has the highest annual frequency (≥ 80%). Its long duration of rise/fall with a consistent rate of change indicates these sites are more likely to occur in large rivers while the highest annual frequency of hydropeaking can pose hydropeaking-induced flow alterations to the aquatic system constantly. G2, large hydropeaking, is characterized by a long-lasting peaking retention (≥ 5 hr) and a higher flow amplitude. The reduction of the annual frequency of hydropeaking is compensated by the increased duration of hydropeaking events. The reduced annual frequency of hydropeaking might reduce the impacts of hydropeaking but the increased flow amplitude can offset this relief to the downstream aquatic systems. G3, supplementary hydropeaking, has the highest frequency of daily peaking events but with a lower magnitude and duration of the individual peaking event. G4, regulated hydropeaking, has the lowest peaking signals among the four groups due to constraints of environment and facilities. G3 has the third strongest impact on the aquatic systems mainly due to its low frequency while G4 should have the least impacts. The four hydropeaking flow regimes were identified from raw time-series flow records are dominant hydropeaking flow regimes for their associated facilities, and it is possible that facilities adopt more than one type of hydropower operation modes.

As for the relative significance of flow-alteration metrics, the duration and frequency of hydropeaking are principal variables governing the classification. Additionally, the magnitude, rate of change and timing of hydropeaking events play less important roles in differentiating hydropeaking flow regimes. By analyzing the seasonality of hydropeaking, it is found that hydropeaking is more frequently conducted in the dry season and drought years. However, sites having strong peaking flow regimes in the dry season tend to have strong hydropeaking in wet season. This study not only provides a valuable tool to help the community to sample high-frequency flow alteration on a large spatial and temporal scale but also created a data analysis framework that can be used worldwide to explore the underlying process especially in regions where documentations of hydropower operation are not well documented. Moreover, the classification of hydropeaking flow provides important insights into the patterns of hydropeaking flow regimes, which is difficult to gain by only knowing the operation modes. Meanwhile, having hydropeaking flow regimes classified into several groups simplified the problem and offers new opportunities to improve the understanding of the flow-ecology relationship. As for the future study topics, the flow-ecology relationship in the setting of hydropeaking flow and the spatial distribution of the classification are highly encouraged.

CRediT authorship contribution statement

Tingyu Li: Conceptualization, Software, Formal analysis, Methodology, Validation, Visualization, Writing - original draft, Writing - review & editing. Gregory B. Pasternack: Conceptualization, Methodology, Supervision, Writing - original draft, Writing - review & editing.

Acknowledgments

This project was supported by the China Scholarship Council for providing Tingyu Li a two-year scholarship and was partially supported by the USDA National Institute of Food and Agriculture, Hatch project number CA-D-LAW-7034-H. We thank Arielle Gervasi for the informal review of the manuscript and Muwei Zheng for his valuable comments on software development. We thank two anonymous reviewers for improving the manuscript with insightful comments.

References

Ashraf, F. B., et al. 2018. "Changes in short term river flow regulation and hydropeaking in Nordic rivers." *Sci Rep* 8 (1):17232. doi: 10.1038/s41598-018-35406-3.

Aghajanzadeh, A., and Therkelsen, P. 2019. "Agricultural demand response for decarbonizing the electricity grid." *Journal of Cleaner Production* 220:827-835. doi: 10.1016/j.jclepro.2019.02.207.
Anindito, Y., et al. 2019. "A new solution to mitigate hydropeaking? Batteries versus re-regulation reservoirs." *Journal of Cleaner Production* 210:477-489. doi: 10.1016/j.jclepro.2019.02.207.
Baker, D. B., et al. 2004. "A new flashiness index: characteristics and applications to Midwestern rivers and streams." *JAWRA Journal of the American Water Resources Association* 40 (2):503-522. doi: 10.1111/j.1752-1688.2004.tb01046.x.
Bejarano, M. D., et al. 2017. "Characterizing effects of hydropower plants on sub-daily flow regimes." *Journal of Hydrology* 550:186-200. doi: 10.1016/j.jhydrol.2017.04.023.
Bejarano, M. D., et al. 2018. "The effects of hydropeaking on riverine plants: a review." *Biol Rev Camb Philos Soc* 93 (1):658-673. doi: 10.1111/brv.12362.
Bevelhimer, M. S., et al. 2015. "Characterizing Sub-Daily Flow Regimes: Implications of Hydrologic Resolution on Ecohydrology Studies." *River Research and Applications* 31 (7):867-879. doi: 10.1002/rra.2781.
Bergen, K. J, et al. 2019. "Machine learning for data-driven discovery in solid Earth geoscience." *Science* 363 (6433):eaau0323. doi: 10.1126/science.aau0323.
Bezdek, J. C. 1973. "Cluster validity with fuzzy sets."
Bezdek, J. C., et al. 1984. "FCM: The fuzzy c-means clustering algorithm." *Computers & Geosciences* 10 (2-3):191-203. doi: 10.1016/0098-3004(84)90020-7.
Bezdek, J. C. 2013. *Pattern recognition with fuzzy objective function algorithms*: Springer Science & Business Media.
Bieri, M. P. 2012. "Operation of complex hydropower schemes and its impact on the flow regime in the downstream river system under changing scenarios." EPFL-LCH.
Borenstein, S., et al. 1995. "Market power in California electricity markets." *Utilities Policy* 5 (3-4):219-236. doi: 10.1016/0957-1787(96)00005-7.
Breiman, L., et al. 1984. *Classification and regression trees*. Belmont, California, USA: Wadsworth International Group.
Capra, H., et al. 2017. "Fish habitat selection in a large hydropeaking river: Strong individual and temporal variations revealed by telemetry." *Sci Total Environ* 578:109-120. doi: 10.1016/j.scitotenv.2016.10.155.
Carolli, M., et al. 2015. "A simple procedure for the assessment of hydropeaking flow alterations applied to several European streams." *Aquatic Sciences* 77 (4):639-653. doi: 10.1007/s00027-015-0408-5.
CAISO, 2004. Ancillary Service Markets [WWW Document]. https://www.caiso.com/Documents/Chapter4_AncillaryServiceMarkets.pdf.
CAISO, 2016. What the Duck Curve Tells Us about Managing a Green Grid [WWW Document]. Calif. Indep. Syst. Oper. https://www.caiso.com/Documents/FlexibleResourcesHelpRenewables_FastFacts.pdf, 8.1.19.
CDEC, 2018. California Data Exchange Center. https://cdec.water.ca.gov/staInfo.html (Accessed 01 2018).
CEC, 2018. California Energy Commission power plant geospatial data. https://cecgis-caenergy.opendata.arcgis.com/datasets/california-power-plants (Accesed 01 2018).

CEC, 2020, California Energy Commission In-State electric generation by fuel type. https://www.energy.ca.gov/data-reports/energy-almanac/california-electricity-data/electric-generation-capacity-and-energy (Accessed 09 2020).

Charmasson, J., and Zinke, P. 2011. "Mitigation measures against hydropeaking effects." *SINTEF Report TR A* 7192.

Corduas, M. 2011. "Clustering streamflow time series for regional classification." *Journal of Hydrology* 407 (1-4):73-80. doi: 10.1016/j.jhydrol.2011.07.008.

Cushman, R. M. 1985. "Review of ecological effects of rapidly varying flows downstream from hydroelectric facilities." *North American journal of fisheries Management* 5 (3A):330-339. doi: 10.1577/1548-8659(1985)5<330:ROEEOR>2.0.CO;2.

Daubechies, I. 1992. *Ten lectures on wavelets*. Vol. 61: Siam.

De'ath, G., and Fabricius, K. E. 2000. "Classification and regression trees: a powerful yet simple technique for ecological data analysis." *Ecology* 81 (11):3178-3192. doi: 10.1890/0012-9658(2000)081[3178:CARTAP]2.0.CO;2.

Greimel, F., et al. 2016. "A method to detect and characterize sub-daily flow fluctuations." *Hydrological Processes* 30 (13):2063-2078. doi: 10.1002/hyp.10773.

Güler, C., and Thyne, G. D. 2004. "Delineation of hydrochemical facies distribution in a regional groundwater system by means of fuzzy c - means clustering." *Water Resources Research* 40 (12). doi: 10.1029/2004WR003299.

Haas, J., et al. 2015. "Grid-wide subdaily hydrologic alteration under massive wind power penetration in Chile." *J Environ Manage* 154:183-9. doi: 10.1016/j.jenvman.2015.02.017.

Harby, A., and Noack, M. 2013. "Rapid flow fluctuations and impacts on fish and the aquatic ecosystem." *Ecohydraulics: an integrated approach*:323-335. doi: 10.1002/9781118526576.ch19.

Hartigan, J. A. 1975. *Clustering algorithms*: John Wiley & Sons, Inc.

Hauer, C., et al. 2012. "Hydro-morphologically related variance in benthic drift and its importance for numerical habitat modelling." *Hydrobiologia* 683 (1):83-108. doi: 10.1007/s10750-011-0942-7.

Hauer, C., et al. 2017. "Longitudinal assessment of hydropeaking impacts on various scales for an improved process understanding and the design of mitigation measures." *Sci Total Environ* 575:1503-1514. doi: 10.1016/j.scitotenv.2016.10.031.

Hauer, C., et al. 2017. "Hydropeaking in regulated rivers-From process understanding to design of mitigation measures." *The Science of the total environment* 579:22. doi: 10.1016/j.scitotenv.2016.11.028.

Kantardzic, M. 2011. *Data mining: concepts, models, methods, and algorithms*: John Wiley & Sons.

Key, T, et al. 2012. Quantifying the value of hydropower in the electric grid. Electric Power Research Inst.(EPRI), Knovville, TN (United States).

Lane, B. A., et al. 2017. "Revealing the diversity of natural hydrologic regimes in California with relevance for environmental flows applications." *JAWRA Journal of the American Water Resources Association* 53 (2):411-430. doi: 10.1111/1752-1688.12504.

Lane, B. A., et al. 2018. "Integrated analysis of flow, form, and function for river management and design testing." *Ecohydrology*:e1969. doi: 10.1002/eco.1969.

Larrieu, K. G., Pasternack, G. B. “2020. Automated analysis of lateral river connectivity and fish stranding risks– Part 1: Review, theory and algorithm.” *Ecohydrology*. doi: 10.1002/eco.2268.
McCune, B., et al. 2002. *Analysis of ecological communities*. Vol. 28: MjM software design Gleneden Beach, OR.
McManamay, R. A., et al. 2015. "Associations among hydrologic classifications and fish traits to support environmental flow standards." *Ecohydrology* 8 (3):460-479. doi: 10.1002/eco.1517.
McManamay, R. A., et al. 2016. "Classification of US Hydropower Dams by their Modes of Operation." *River Research and Applications* 32 (7):1450-1468. doi: 10.1002/rra.3004.
Meile, T., et al. 2011. "Hydropeaking indicators for characterization of the Upper-Rhone River in Switzerland." *Aquatic Sciences* 73 (1):171-182. doi: 10.1007/s00027-010-0154-7.
Melcher, A. H., et al. 2017. "Drawing together multiple lines of evidence from assessment studies of hydropeaking pressures in impacted rivers." *Freshwater Science* 36 (1):220-230. doi: 10.1086/690295.
Moog, O. 1993. "Quantification of daily peak hydropower effects on aquatic fauna and management to minimize environmental impacts." *River Research and Applications* 8 (1 - 2):5-14. doi: 10.1002/rrr.3450080105.
Moreira, M., et al. 2019. "Ecologically-based criteria for hydropeaking mitigation: A review." *Science of The Total Environment* 657:1508-1522. doi: 10.1016/j.scitotenv.2018.12.107.
Poff, N. L, John C. S. 2016. "How dams can go with the flow." *Science*. doi: 10.1126/science.aah4926
Olden, J. D., et al. 2012. "A framework for hydrologic classification with a review of methodologies and applications in ecohydrology." *Ecohydrology* 5 (4):503-518. doi: 10.1002/eco.251.
Palmer, M. A., et al. 2005. "Standards for ecologically successful river restoration." *Journal of applied ecology* 42 (2):208-217. doi: 10.1111/j.1365-2664.2005.01004.x.
Parasiewicz, P., et al. 1998. "The effect of managed hydropower peaking on the physical habitat, benthos and fish fauna in the River Bregenzerach in Austria." *Fisheries Management and Ecology* 5 (5):403-417. doi:10.1046/j.1365-2400.1998.550403.x.
Poff, N. L., et al. 1997. "The natural flow regime." *BioScience* 47 (11):769-784. doi: 10.2307/1313099.
Poff, N. L., and Ward, J. V. 1989. "Implications of streamflow variability and predictability for lotic community structure: a regional analysis of streamflow patterns." *Canadian journal of fisheries and aquatic sciences* 46 (10):1805-1818. doi: 10.1139/f89-228.
R Core Team, 2020. “R: A language and environment for statistical computing.” R Foundation for Statistical Computing, Vienna, Austria.Reichstein, M., et al. 2019. "Deep learning and process understanding for data-driven Earth system science." *Nature* 566 (7743):195-204. doi:10.1038/s41586-019-0912-1.
Resh, V.H., Brown, A.V., Govich, A.P., Gurtz, M.E., Li, H.W., Minshall, G.W., Reice, S.R., Sheldon, A.L., Wallace, J.B., Wissmar, R.C., 1988. The role of disturbance in stream ecology.. Journal of the North American benthological society 7 (4), 433–455. doi:10.2307/1467300.
Richter, B. D., et al. 1996. "A method for assessing hydrologic alteration within ecosystems." *Conservation biology* 10 (4):1163-1174.

Ross, T. J. 2005. *Fuzzy logic with engineering applications*. Vol. 2: Wiley Online Library.

Sauterleute, J. F., and Charmasson, J. 2014. "A computational tool for the characterisation of rapid fluctuations in flow and stage in rivers caused by hydropeaking." *Environmental Modelling & Software* 55:266-278. doi: 10.1016/j.envsoft.2014.02.004.

Schülting, L., et al. 2016. "Effects of hydro-and thermopeaking on benthic macroinvertebrate drift." *Science of The Total Environment* 573:1472-1480. doi: 10.1016/j.scitotenv.2016.08.022.

Sergeant, C. J., et al. 2020. "A classification of streamflow patterns across the coastal Gulf of Alaska." *Water Resources Research*. doi: 10.1029/2019wr026127.

Spurgeon, J. J., et al. 2016. "Multi-scale Approach to Hydrological Classification Provides Insight to Flow Structure in Altered River System." *River Research and Applications* 32 (9):1841-1852. doi: 10.1002/rra.3041.

Thompson, L. C., et al. 2010. "Longitudinal movement of fish in response to a single-day flow pulse." *Environmental Biology of Fishes* 90 (3):253-261. doi: 10.1007/s10641-010-9738-2.

USGS, 2018. GAGES-II: Geospatial Attributes of Gages for Evaluating Streamflow. https://water.usgs.gov/GIS/metadata/usgswrd/XML/gagesII_Sept2011.xml (Accessed 01 2018).

Wu, F. C., et al. 2015. "Assessment of flow regime alterations over a spectrum of temporal scales using wavelet‐based approaches." *Water Resources Research* 51 (5):3317-3338. doi: 10.1002/2014WR016595.

Young, P. S, et al. 2011. "Hydropower-related pulsed-flow impacts on stream fishes: a brief review, conceptual model, knowledge gaps, and research needs." *Reviews in Fish Biology and Fisheries* 21 (4):713-731. doi: 10.1007/s11160-011-9211-0.

Zimmerman, J. KH., et al. 2010. "Determining the effects of dams on subdaily variation in river flows at a whole‐basin scale." *River Research and Applications* 26 (10):1246-1260. doi: 10.1002/rra.1324.

Zolezzi, G., et al. 2009. "Assessing hydrological alterations at multiple temporal scales: Adige River, Italy." *Water Resources Research* 45 (12). doi: 10.1029/2008wr007266.